Effects of Surface Roughness Length on the Atmospheric Circulation in a Tidally-Locked Planet

A Thesis

submitted to

Indian Institute of Science Education and Research Pune

in partial fulfillment of the requirements for the

BS-MS Dual Degree Programme

by

Shijil Amin P Umer

Indian Institute of Science Education and Research Pune

Dr. Homi Bhabha Road,

Pashan, Pune 411008, INDIA.

May, 2025

Supervisor: Dr. Joy Merwin Monteiro

Expert: Dr. Ravi Kumar Kopparapu

Certificate

This is to certify that this dissertation entitled 'Effects of Surface Roughness Length on the Atmospheric Circulation in a Tidally-Locked Planet' towards the partial fulfilment of the BS-MS dual degree programme at the Indian Institute of Science Education and Research, Pune represents study/work carried out by Shijil Amin P Umer— at Indian Institute of Science Education and Research under the supervision of Dr. Joy Merwin Monteiro, Assistant Professor, Department of Earth and Climate Science, during the academic year 2020-2025.

Dr. Joy Merwin Monteiro

Ravi Kopparapu

Dr. Ravi Kumar Kopparapu

Committee:

Dr. Joy Merwin Monteiro

Dr. Ravi Kumar Kopparapu

This thesis is dedicated to the shape of things to come.

Declaration

I hereby declare that the matter embodied in the report entitled 'Effects of Surface Roughness Length on the Atmospheric Circulation in a Tidally-Locked Planet', are the results of the work carried out by me at the Department of Earth and Climate Science, Indian Institute of Science Education and Research, Pune, under the supervision of Dr. Joy Merwin Monteiro and the same has not been submitted elsewhere for any other degree.

Shijil Amin P Umer

Dr. Joy Merwin Monteiro

Acknowledgments

I would like to thank my supervisor Dr. Joy Merwin Monteiro and my thesis expert Dr. Ravi Kumar Kopparapu for their guidance, support and the many invaluable conversations shared. I would also like to thank Dilip V for his help in tackling some of the theoretical aspects related to my project.

On a less formal note, I couldn't have asked for better friends than the ones I have made in college. They've supported me through the meat grinder that was the last few (too many) years. The never-missed weekly conversations with Ananthu, the everlooming threatening existence of Kashika and the constant spiritual presence of Jo have all helped keep sane. I'm glad for the times shared with all friends- past and present.

Special shout-out to my therapist and psychiatrist.

Has been quite the experience really. I'm definitely happy to have gone through it and come out a different, almost unrecognizable person.

Tempus fugit, after all.

Abstract

With the advent of advanced observational techniques in characterizing exoplanetary atmospheres, it has become necessary to model the general circulation dynamics of these atmospheres- taking into account their spectroscopically identified composition, external forcing, orbital dynamics etc. to enable inverse modelling of the planetary conditions and their underlying physics. Capturing the nuances of atmospheres and forcings that are alien to planets in our solar system would shed more light into the more generalized physical processes that governed the formation of our planetary system, the Earth and its atmosphere.

Hence exoplanetary sciences could provide us with a way to understand our own past, and possibly our future.

Many projects have been undertaken by people working in this field to resolve the effect of each parameter such as orbital distance, rotation rate, stellar insolation, cloud distribution, etc. in shaping the atmospheric circulation of exoplanets and how they may be interpreted from observational data. For the purpose of this thesis, we have identified a research gap in resolving the effect of surface roughness length on the atmospheric dynamics of a tidally-locked exoplanet. Surface roughness being a reasonable representative variable of terrain, we hope this simple thesis project could contribute towards more advanced studies that may help in quantifying the effect of surface friction and terrain on observable atmospheric features.

The scope of this project- in the context of atmospheric science- is limited to understanding how the planetary boundary layer functions, how variations in the surface roughness length changes the circulation, and how such changes are propagated through the atmosphere via eddies.

Contents

List of Figures

Chapter 1

Introduction

Over the last few decades, advances in observational astronomy and engineering have helped in the survey and discovery of a wide variety of planetary bodies and their properties. Space-based observatories such as NASA's James Webb Space Telescope (JWST) launched in 2021 offer a great vantage point to glance into the world of extrasolar planets and infer their properties (Seidel et al. 2023). In doing so, we are overcoming the limited sample size of eight planets offered by our solar system and developing a more fundamental understanding of the formation and evolutionary processes of planetary bodies and their atmospheres. Several methods such as transit spectroscopy, direct imaging, phase curve modelling, high-dispersion spectroscopy etc (Crossfield 2015). are employed to find the spectral and thermal properties of a planet orbiting a star. The presence of different chemical compounds in gaseous forms or their condensates in the form of clouds or hazes have significant impacts on the observable properties and spectra of exoplanets (Feinstein et al. 2023). With the help of forward and inverse atmospheric modelling (Crossfield 2015, Madhusudhan et al. 2014), we are often able to reach a reasonable consensus on the climate and surface properties of these planets. Hence, three-dimensional General Circulation Models (GCM) are of great importance to gauge the dynamics of a planet and its atmosphere.

A significant number of discovered exoplanets are believed to be terrestrial with the possibility of tidal locking- where the tidal forces of the star wears down the planet's rotation until the time taken to complete one rotation about its axis becomes equal to its orbital period around the host star. Such a scenario is also referred to as synchronous rotation. Tidal-locking would imply that one hemisphere of the planet would be permanently facing the star (day-side) while the other faces away (night-side). From a very rudimentary perspective of radiative balance, this would mean the night-side acts as *radiator fin* which helps remove the excess heat received via the day-side insolation. Studying how such planets can sustain an atmosphere could give insight into atmospheric processes and effects that would be alien to Earth's climate regimes. One can expect the atmospheric circulation to carry significant amounts of energy from the perpetual day-side to the night-side in order to sustain an atmosphere because should the continuous loss of temperature from the night-side lead to condensation of all gaseous components, the planet would face an atmospheric collapse. Hence mechanisms of energy transport are of great interest to us and in this project, we explore the role of the planetary boundary layer in helping to sustain a stable surface temperature profile and how variations in the surface roughness length can lead to significant changes in the dynamics of the atmosphere.

Surface roughness length is a parameter used in meteorology to help calculate the near-surface wind speeds in climate models. When following the logarithmic wind profile as suggested by the Monin-Obukhov Similarity (MOS) theory (Monin and Obukhov 1954), the surface roughness length corresponds to the height at which the mean wind speeds become zero in neutral atmospheric conditions. The terrain plays a very critical role in determining the value of the surface roughness length of a region. A flat, featureless terrain such as that of a very calm ocean would correspond to a low surface roughness length of the order of 0.0001 meters while a terrain with a homogeneously distributed forest would have a roughness of the order of 1 (Wieringa 1992). Chen et al. 2007 shows how the position of the surface westerlies (and the associated eddy-driven midlatitude jet) is sensitive to surface friction. In our experiment we try to modulate this parameter to determine its effects on the circulation in the presence of a tidally-locked solar forcing.

Although ocean circulations play a significant role in the energy transport budget of an aqua-planet (Y. Hu and Yang 2014), in this project we will be exclusively focusing on the role of the atmosphere in transporting energy through an AGCM (Atmospheric General Circulation Model) with the use of a 'Slab Ocean' devoid of any circulations. I will be using the **climt** (Climate Modelling and Diagnostics Toolkit, Monteiro, McGibbon, et al. 2018) numerical modelling library in python to construct the GCM, subject to a simple Grey radiation scheme.

In this thesis, we hope to tackle the following aspects:

- Understanding and writing a boundary layer component capable of handling the extremely stable atmospheric conditions expected in a tidally-locked planet
- Stabilizing a tidally locked GCM for varying surface roughness lengths
- Analyzing changes in the zonal-mean circulation as the surface drag is changed.

Chapter 2

Methods and Theoretical Background

During the course of the project, certain components of the model had to be modified to deal with the extreme forcing scenarios of a tidally-locked system. In this chapter, we will explore the general set up of the model, how it is tailored to fit our conditions, and the theoretical background of the modified model components which enable us to capture the dynamics of our planet's atmosphere in a numerically stable and physically reasonable manner.

We will start with a brief explanation of how the *climt* package works, the physical phenomenon represented by the components, the changes made to make the GCM capable of simulating a tidally-locked atmosphere, and the overall explanation of the experimental setup.

2.1 The GCM Setup

I use the *climt* (Climate Modelling and Diagnostics Toolkit) package which uses the *sympl* (System for Modelling Planets) framework (Monteiro, McGibbon, et al. 2018) to set up the three-dimensional General Circulation Model that will be used for the experiments.

climt utilizes multiple components that are either purely Python-based or wrapped Fortran packages to compute the effects of different atmospheric phenomena. For my project, the GCM is set up using simple components which serve the function of modelling the following aspects:

- Convection: A simple convection scheme which is designed based on Emanuel and Živković-Rothman 1999.
- Slab Ocean Surface: To model a static ocean devoid of any dynamics which is used to calculate the surface energy balance and the surface temperature.
- Insolation: A simple insolation package to calculate the zenith angles and received solar influx for each grid point based on latitude and longitude. In our case the insolation is set to model a tidally-locked system which receives 900 W/m^2 of insolation at the substellar point.
- Grey Longwave Radiation scheme to calculate the radiative tendencies due to a simple Grey atmosphere. The optical depth is set based on Frierson et al. 2006.
- Boundary Layer: To account for the planetary boundary layer (PBL) dynamics such as the exchange of sensible and latent heat fluxes between the surface and atmosphere, to modulate the effects of surface drag, and to account for the turbulent eddies inherent to the PBL. Developing a boundary layer scheme suitable for modelling a tidally-locked atmosphere was quite a challenging part of my thesis and the work put towards this task is described in detail in the following section.

The dynamics of the model is stepped forward in time using a spectral dynamical core derived from the General Forecast System using an implicit–explicit total variation diminishing Runge–Kutta time stepper while the tendencies are stepped using a forward Euler scheme.

2.2 The Planetary Boundary Layer

The planetary boundary layer (PBL) often refers to some of the lowermost regions of the atmosphere, which are directly under the influence of the frictional and radiative forcings offered by the planet's surface and respond to these forcings in about hour-long timescales or less (Stull 2012). Apart from mean winds which play a major role in horizontal advection, turbulence - caused by buoyant thermals or friction induced wind shear near the surface- is one of the most important mechanisms at play in the boundary layer which helps in transporting heat, momentum etc. It is stronger than molecular diffusion in transporting measurable quantities up and down the boundary layer. Effectively, turbulence is the 'coupling' mechanism between the surface and the free atmosphere and if turbulence were to collapse, the planetary surface and the atmosphere would be completely energetically decoupled. This is one of the most interesting themes that would be tackled in this project as we explore different boundary layer formulations, its limitations when it comes to a collapse of turbulence, and how we can mathematically circumvent this problem.

2.2.1 The Drag Formulation

The exchange of heat, momentum, and moisture between the surface and the atmosphere is modelled by the standard drag laws (Frierson et al. 2006). Surface stress, sensible heat flux and evaporation respectively are given by:

$$\tau = \rho C v_a^2 \tag{2.1}$$

$$S = \rho c_p C v_a \Delta\theta \tag{2.2}$$

$$E = \rho C v_a (q - q_s^*) \tag{2.3}$$

where c_p is the heat capacity at constant pressure, $\Delta\theta$ is the difference between the potential temperature of the layer and the surface, q_s^* is the saturation specific humidity at the surface temperature while v_a, rho, and q_a are the horizontal wind, density, and specific humidity at the lowest model layer.

At the beginning of the project, we used a simple boundary layer scheme outlined in Frierson et al. 2006 which modulate the drag coefficient (C) and diffusivity of the boundary layer based on the Richardson number as follows

$$C = k^2(ln\frac{z}{z_o})^{-2} \quad \text{for } Ri_a < 0 \tag{2.4}$$

$$C = k^2(ln\frac{z}{z_o})^{-2}(1 - \frac{Ri_a}{Ri_c})^2 \quad \text{for } 0 < Ri_a < Ri_c \tag{2.5}$$

$$C = 0 \quad \text{for } Ri_a > Ri_c \tag{2.6}$$

where Ri_c is a critical Richardson number, Ri_a is the Richardson number calculated between the surface and the lowest modelled layer, z is the height/thickness of the lowest layer, and z_o is the roughness length.

The bulk Richardson number- a dimensionless parameter measuring the ratio of the buoyancy to the turbulent shear- is calculated as:

$$Ri = gz\frac{\Delta\theta}{\theta_s u^2} \tag{2.7}$$

with θ_S being the surface virtual temperature and $\Delta\theta$ the virtual potential temperature difference between the surface and the layer. The value of Ri becomes positive for stable boundary layer conditions with increasing virtual potential temperature due to the positive buoyancy (we take the convention that a stable atmosphere has a positive buoyancy and an unstable one has a negative buoyancy) and negative for unstable boundary layer conditions where the virtual potential temperature drops as one moves upwards.

Once the GCM was set up for a test run, we noticed that the surface temperatures in the equatorial night-side dropped to extremely low values below 100 K and was nearing absolute zero as the model progressed- resulting in a crash. Upon taking a closer look of the surface fluxes and temperatures of the surface as well as the lowest modelled layer, it was discovered that beyond a certain point of criticality in the run, all exchange of sensible heat fluxes between the surface and the lowest modelled layer completely shut down (Figure 2.1).

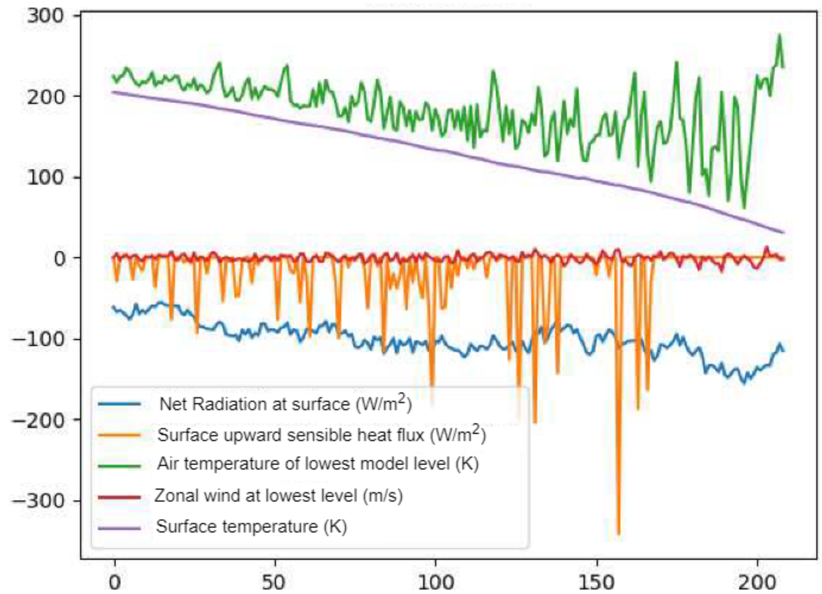

Figure 2.1: Time series representation showing the atmosphere and surface decoupling at the antistellar point in the GCM. The sensible heat fluxes (Orange) can be seen to go to zero following with the air temperature (Green) and Surface temperature (Purple) fluctautes and diverges.

Once the sensible heat fluxes stopped working, the energy balance became purely radiative with the surface losing its heat in the form of outgoing longwave radiation to space.

This can be pinpointed to the drag coefficient going to zero as the Richardson number goes beyond the assigned critical value as shown in equation 2.6. Due to the tidal-locking that we impose on the GCM, the night-side of the planet continually loses heat in the form of outgoing longwave radiation so it relies exclusively on the transfer of heat from the atmosphere (advectively brought to the night-side from the warmer day-side) to the surface. The nocturnal inversion of the stable boundary layer grows stronger as the surface temperature drops. This increase in $\Delta\theta$ proportionally increases the value of the Richardson number (see equation 1.7) and once the critical value is crossed, the drag coefficient becomes zero, energy exchange at the surface layer shuts down and the planetary surface becomes energetically decoupled from the atmosphere. The surface would then simply lose heat radiatively as the modelled temperature plummets towards absolute zero.

The inability of the Frierson scheme to tackle extremely stable boundary layer conditions that would be prevalent in the permanent night-side of a tidally-locked planet leads us to seek other formulations. Over the years, quite a number of alternatives have been provided to address very similar issues in forecast models. Zheng et al. 2017 suggests that the collapse of turbulence (and thus the surface fluxes) is due to the sub-grid scale non-turbulent motions (such as cold-air drainage)- which are generally omitted in numerical models- becoming non-negligible in extremely stable conditions. A runaway effect of surface temperature could be countered by modelling the ground heat flux from the soil temperature gradient or by formulating the drag such that the sensible heat flux transfer from atmosphere to ground is more strongly proportional to the temperature difference, allowing for a possible equilibrium to be attained. The former solution requires accounting for the soil temperature structure but the latter is more achievable by considering a change in the formulation of the drag coefficient.

Zheng et al. 2017 tries to curb this issue with the stable surface layer for the NCEP Global Forecast System by imposing a constraint on the z/L stability parameter and introducing a seasonality to the roughness length. This, while solving their problem of cold-bias (of the 2-m air temperature) in the forecast model, cannot be an appropriate solution for the runaway effects in the permanent night-side of our simple model.

Jean-Francois Louis' 1979 paper (Louis 1979) offers a parametric method to simulate vertical eddy fluxes of heat, momentum and moisture in a 10-day forecast model. Louis appears to have made similar conclusions about the limitations of using a quadratic scaling for the drag coefficient on the Richardson number and says that once bulk Richardson number exceeds the critical value, it leads to energetic decoupling between the atmosphere and surface. Carson and Richards 1978 suggests increasing the critical value of the Richardson number in hopes of extending the regime of the model's stability however, in applying this, we found that the GCM simply takes longer to reach the inevitable decoupling. Also to note is that increasing the critical value by a very large factor should in theory indefinitely prolong the decoupling but this also gives highly unphysical and overestimated values for drag (and thus the eddy fluxes) at highly stable conditions.

Another possible solution suggested by Kondo et al. 1978 and applied in Louis 1979 is to change the linear flux-profile relationship generally followed in stable conditions to tend to an asymptotic value at high Richardson numbers. To do this, the neutral value of the drag coefficient (i.e., the value for Ri=0) is scaled using a function F which varies based on Ri as:

A very similar formulation is also offered by Long 1986. The stable conditions in the 'E2' boundary layer scheme of the Medium Range Forecast Model (MRF86) is segmented into four domains- weakly stable, mildly stable, strongly stable, and non-turbulent. To expand the stability regime and to simplify the calculations, an asymptotic relationship similar to equation 2.10 is proposed by changing the flux-profile relationship.

$$C = C_0 F \tag{2.8}$$

$$F = 1 - b\frac{Ri}{1 + c\sqrt{Ri}} \quad \text{for Ri} < 0 \tag{2.9}$$

$$F = \frac{1}{(1 + b'Ri)^2} \quad \text{for Ri} > 0 \tag{2.10}$$

$$C_0 = k^2(ln\frac{z}{z_o})^{-2} \quad \text{is the neutral drag coeff.} \tag{2.11}$$

$$c = 7.4bC_0 \tag{2.12}$$

It is suggested to take the constants b = 2b' = 9.4 in order to maintain mathematical continuity for the first derivative of F between the stable and unstable conditions.

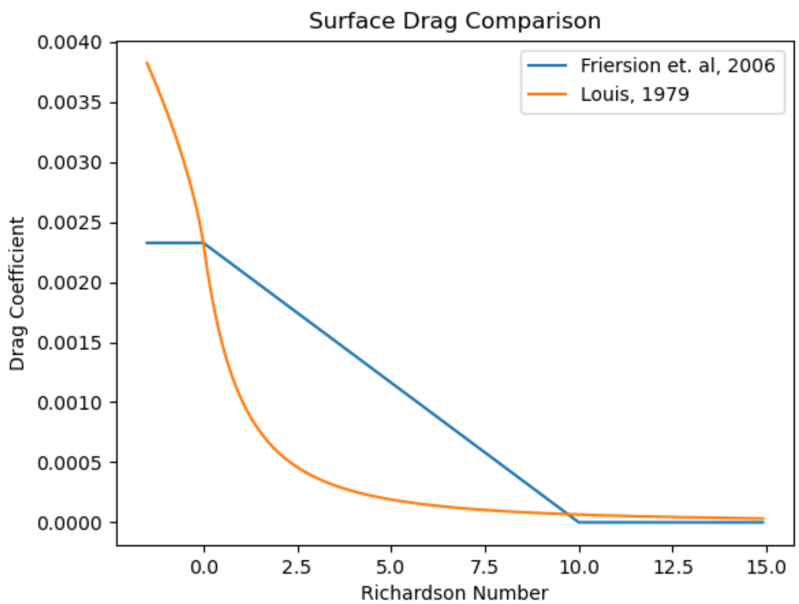

Figure 2.2: Comparative plot of the surface drag formulation in the 2 papers. The surface roughness length z_o is assumed to be 0.001 m in both cases.

2.2.2 Diffusive Modelling of Eddy Fluxes

It is found that by employing this asymptotic curve for drag, and thus the surface fluxes, we avoid a decoupling of the surface and the atmosphere. However, in order to ensure that a model realistically runs to equilibrium, one needs to look at how the diffusion is modelled as well. Diffusion plays a very important role in helping maintain the night-side surface temperatures by bringing heat down to the lower levels of the boundary layer in the form of diffusive eddy fluxes. The previously discussed changes to drag may have avoided decoupling between the surface and the atmosphere within the boundary layer but if diffusion (and how we define the extent of the boundary layer) is not handled cautiously, the entirety of the boundary layer could end up decoupled from the free atmosphere while modelling a tidally-locked scenario.

In the Frierson et al. 2006 formulation, diffusivity (K) above the surface layer is modelled as:

$$K = K_b(z) \quad \text{for } z < f_b h \tag{2.13}$$

$$K = K_b(f_b h)\frac{z}{f_b h}[1 - \frac{z - f_b h}{(1 - f_b)h}]^2 \quad \text{for } f_b h < z < h \tag{2.14}$$

where K_b- the surface layer diffusion- is taken to be consistent with simplied Monin-Obhukov theory as:

$$K_b(z) = \kappa u_a \sqrt{C} z \quad \text{for } Ri_a < 0 \tag{2.15}$$

$$K_b(z) = \kappa u_a \sqrt{C} z[1 + \frac{Ri}{Ri_c}\frac{ln\frac{z}{z_o}}{1 - \frac{Ri}{Ri_c}}]^{-1} \quad \text{for } Ri_a > 0 \tag{2.16}$$

Here κ is vorn Karman constant, Ri_a is the Richardson number of the lowest modelled layer, and C is the drag coefficient which is formulated as equations 2.4-2.6 in the Frierson scheme.

The height of the boundary layer is calculated using a critical value for the Richardson number. Do note that this critical Richardson number is not the same one we have discussed earlier, this is simply the Richardson number calculated for each modelled level of the atmosphere relative to the surface. For a given column, we determine the height of the boundary layer to be the height of the lowest modelled layer with the Richardson number greater than the critical value that we have set.

Since the Frierson diffusivity is scaled to the height of the boundary layer- with the diffusivity increasing from a value at the surface layer and tapering off to zero at the top (as seen in Figure 2.3)- the effect of the eddy fluxes would be limited entirely to the height of the boundary layer. If we were to set the critical value of the Richardson number to be 1, the height of the night-side stable boundary layer would be about 200 meters. But the build-up of heat (advected from the day-side) above the boundary layer would imply that the Richardson number for these layer(s) immediately above the boundary layer would grow higher as the model runs progress. This would mean that it would be harder for the night-side columns to expand its boundary layer and allow for the diffusion of the heat towards the surface. So, even though the surface and atmosphere would not get decoupled, the boundary layer and the free atmosphere definitely can. This leads to another runaway effect where the surface simply radiates away all its heat and no equilibrium can be attained using the model.

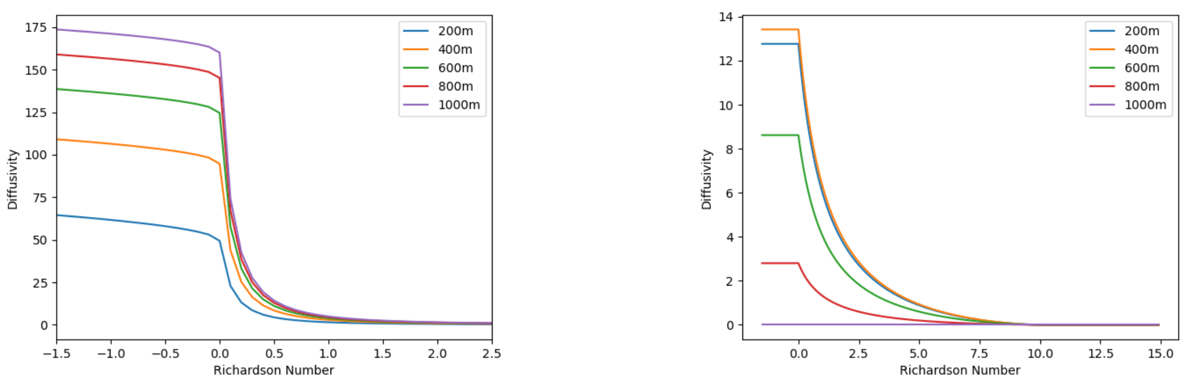

(a) Louis, 1979

(b) Frierson et. al, 2006

Figure 2.3: Diffusivity of each formulation at different altitudes. The roughness length in both cases is presumed to be 0.01m

Louis 1979 once again offers a solution to this by modelling the diffusive eddy fluxes not just in an arbitrarily determined boundary layer but throughout the atmosphere. It is formulated such that the diffusivity values are two or three orders of magnitude smaller than the values near the surface. The diffusion coefficient, dependent on height, shear and stability, is calculated as:

$$K = l^2 \left|\frac{\Delta u}{\Delta z}\right| F(Ri) \tag{2.17}$$

$$l = \frac{kz}{1 + \frac{kz}{\lambda}} \tag{2.18}$$

where l is the mixing length (Blackadar 1962), k is the von Karman constant, λ is an adjustable parameter and F is the function discussed earlier in equations 2.9, 2.10. However some key variations are made to how the Richardson number and the constant c (equation 2.12) is calculated:

$$Ri = g\Delta z \frac{\Delta\theta}{\theta_s \Delta u^2} \tag{2.19}$$

$$c = 7.4 l^2 b \frac{[(z + \frac{\Delta z}{z})^{1/3} - 1]^{3/2}}{z^{1/2}\Delta z^{3/2}} \tag{2.20}$$

We also change how the stability is determined for each grid point. While previously we took the Richardson number of the lowermost layer to determine the stability of the entire column and applied the same formula for diffusion throughout, here we check the Ri value for each layer in a column and depending on whether it is positive or negative, we apply correct form of F to calculate the diffusion coefficient at that particular level in the column. The reason we do this is because since we now don't explicitly restrict the boundary layer to a certain height, we need to account for the highly positive values of the Richardson number for the upper levels of the atmosphere. If we determine an entire column to be unstable and try to compute the diffusivity for a level with highly positive Ri using equation 2.9 (which is used for $Ri < 0$), we will end up obtaining a negative value for diffusivity– which is unphysical.

Do note that despite the mixing length l increasing with height, the diffusivity decreases with height due to the stable nature of the free atmosphere ($Ri > 0$) resulting in the value of $F(Ri) << 1$ above the boundary layer of the atmosphere. Typically K is a few orders of magnitude greater in the unstable boundary layer than in the free atmosphere and only in cases of very high shear will K obtain a non-negligible value in the upper levels. This is tolerable since we can expect high diffusive action in regions of high shear no matter where it is in the atmosphere. Hence, in a certain way, the Louis formulation helps tackle tropospheric diffusion as well.

2.3 The Experiment

Now that we have established the efforts made to set up the GCM in the previous 2 sections, I will give a brief description of the experiment that I have conducted to gauge the effects of varying surface roughness length in the atmospheric circulation and energy distribution.

I have produced three model runs of varying surface roughness length (z_o) of 0.01 m, 0.1 m and 1 m. These changes ranging over three orders of magnitude should affect both the surface drag as well as the behaviour of the diffusively modelled turbulent eddies of the boundary layer.

The runs are produced with the ocean mixed layer thickness (which reflects the heat capacity of the surface) to be 20 meters and the insolation and the substellar point to be 900 W/m^2. The model is stepped forward in time in steps of 10 minutes each- a value chosen to be suitable for all the components used and low enough to avoid problems due to highly discretised time steps. The insolation value is selected to be 900 W/m^2 to avoid any runaway effects due to higher or lower insolation in an optically thick grey atmosphere. The rotation rate of the planet is considered to be same as that of the earth at one rotation every 24 hours. But we impose the tidal locking condition by implying that it constitutes one orbit around the host star every 24 hours. It should be admitted that while there might be a disparity between the insolation and the orbital radius (as implied by the orbital period of 24 hours), the aim of this experiment is to simply capture the effects of roughness length and it is not fully intended to represent reality of orbital mechanics in the strictest form. I hope to analyze the cases with realistic orbital parameters and insolation as a function of these parameters in the future.

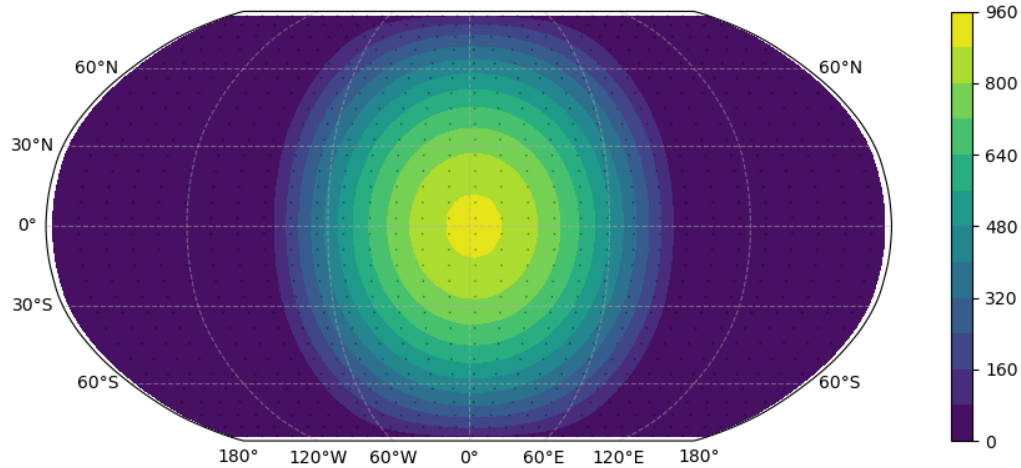

Figure 2.4: Insolation profile (W/m^2) at the top of the atmosphere.

The radius of the planet, surface acceleration due to gravity, Coriolis parameter are all same as that of the Earth. The surface of the planet is gridded into 64 $\times$ 30 grids (zonally $\times$ meridionally) leading to an effective resolution of approximately $5.625^o \times 6^o$. The model computes 28 vertical levels which are linearly interpolated (using the SciPy 'interp1d' class) and re-gridded into 23 isobaric levels later for ease of analysis (Virtanen et al. 2020).

The runs for each surface roughness value is spun up from an isothermal atmosphere of 290 K for a period of 6 years until the net flux at the top of the atmosphere equilibriates to a small value. And to further ensure an equilibriated state for the system, each run is simulated for atleast a 30 year span. The data obtained is analyzed and discussed in the following chapter.

Chapter 3

The General Circulation

3.1 General Features of Profiles

The day-side temperature profile shows a moist adiabatic profile extending upto a tropopause at about 60-50 hPa while the night-side temperature profile is characterize by a strong inversion at around the 700-600 hPa level which marks the top of the night-side boundary layer. Above this level, the temperature tends to be zonally quite uniform, especially in the lower latitudes despite the zonally varying insolation profile that we use (Figure 3.4). This is in agreement with the Weak Temperature Gradient (WTG) theory for tidally-locked planets (Pierrehumbert and Hammond 2019).

The location of maximum surface temperature is not directly beneath the substellar point but shifted off-equator and west of the substellar point. The surface temperature in the mid-latitudes trail off eastward into the night side and the night-side equatorial region is generally colder than the higher latitudes.

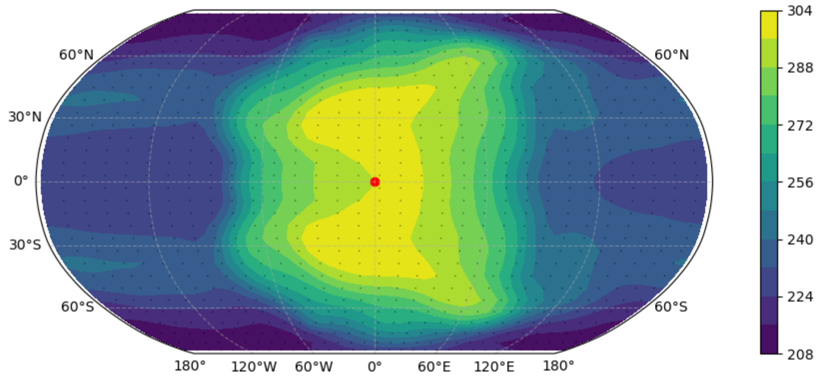

(a) 1 m

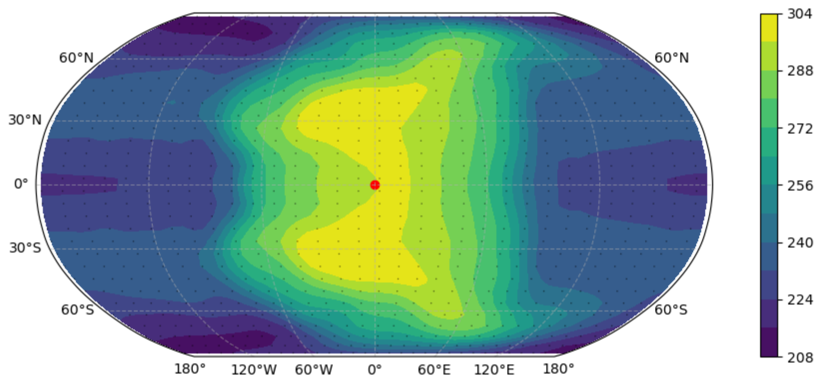

(b) 0.1 m

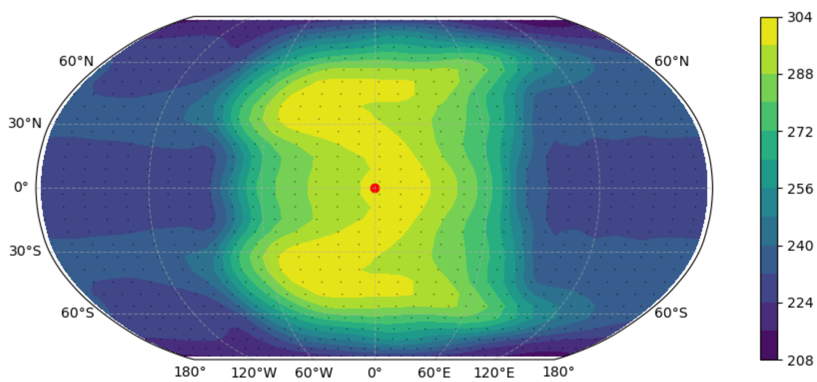

(c) 0.01 m

Figure 3.1: Surface temperature profiles (in Kelvin). Red dot marks the substellar point

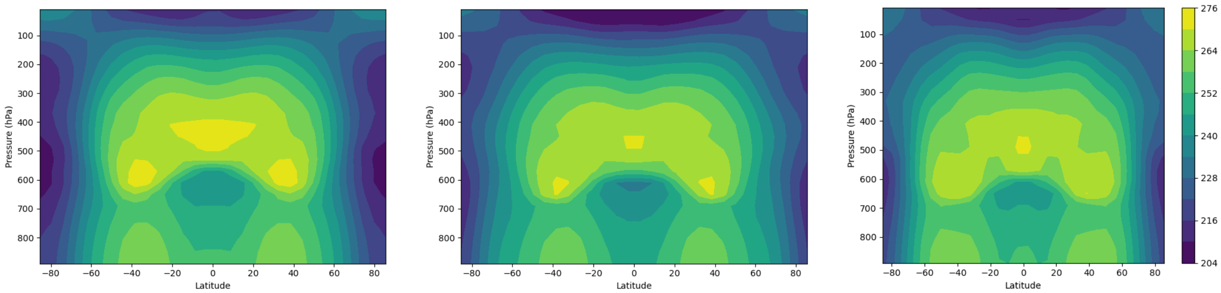

(a) 1 m (b) 0.1 m (c) 0.01 m

Figure 3.2: Zonal-mean air temperature profiles (in Kelvin)

In all three runs, we observe westerly jets in the mid-latitudes and mean easterly flow in the equatorial and subtropical regions (with a strong mid-tropospheric equatorial mean westerly flow in the 0.01m scenario exclusively- Figure 3.3-c). The variations in the location and/or strength of these jets will be discussed in the next section.

The origin of the mid-latitude jets are yet to be identified. The study of the transience observed during the spin-up of the model is beyond the scope of the thesis and we hope to better understand the formation process and timeline of the jets in the model in the future. But for the purpose of this thesis, we will restrict ourselves to understanding the zonal momentum budget and the transport of momentum by eddies.

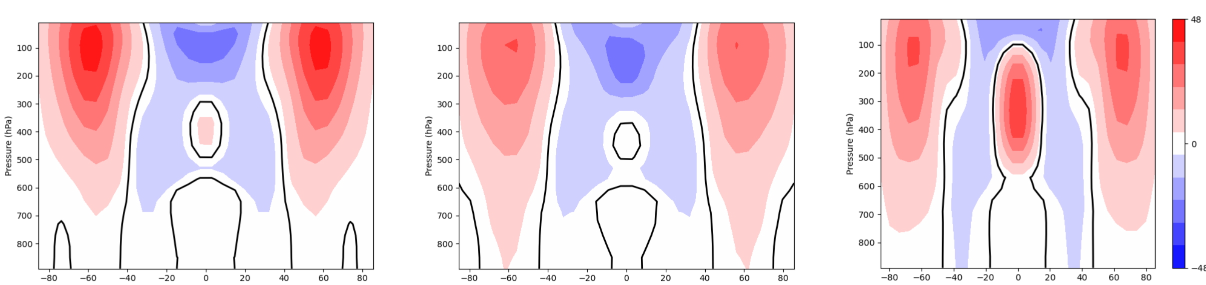

(a) 1 m (b) 0.1 m (c) 0.01 m

Figure 3.3: Zonal-mean Zonal Winds for 1m, 0.1m and 0.01m runs. Zero lines are contoured in black. Colourbar indicates windspeeds in m/s

3.2 Inter-Run Variations

Upon comparing the climatological mean fields of the five completed runs, the impact of increasing surface roughness length on the atmospheric circulation can be drawn:

- There is a strong super-rotating mean flow in the equatorial mid-tropospheric level which disappears as the friction increases.
- The cores of the subtropical westerly jets shifts equator-ward with increasing friction.
- The equatorial upper-tropospheric easterly jet cores become faster proportional to the surface roughness.

The changes in the position of mid-latitude jets are in agreement with the studies conducted by Chen et al. 2007, where it was demonstrated that the circulation– in particular, the location of the surface westerlies– are sensitive to the surface drag. They used a very simple model for the atmospheric drag while we have more complex method of accounting for the turbulent eddies and the surface friction but nonetheless the observed behaviour of the location of the jets are in line with the changes expected as a function of surface friction.

It is clear that modulating the surface roughness causes quite a significant change in the circulation of a tidally-locked atmosphere. But the question remains as to what energy or momentum transfer pathways are most affected by the change in surface friction or atmospheric drag to bring about these considerable changes in the circulation.

The immediate effects of surface drag (Equation 2.1) on the lowest modelled layer would modulate the low-level shear, and thus the momentum fluxes generated by the turbulent eddies. One can expect the effects of this to be most prominent on the permanent day-side of the planet due to the strong atmospheric instability present in this region (diffusive fluxes are strongest in an unstable atmosphere- Figure 2.3).

The maximum and minimum surface temperature of the climatologies appear to be inversely proportional to the surface roughness while in the case of the wind-speeds, the maxima of the westerly winds and the maxima of the easterly winds are directly proportional to the surface roughness lengths (see Figure 3.5).

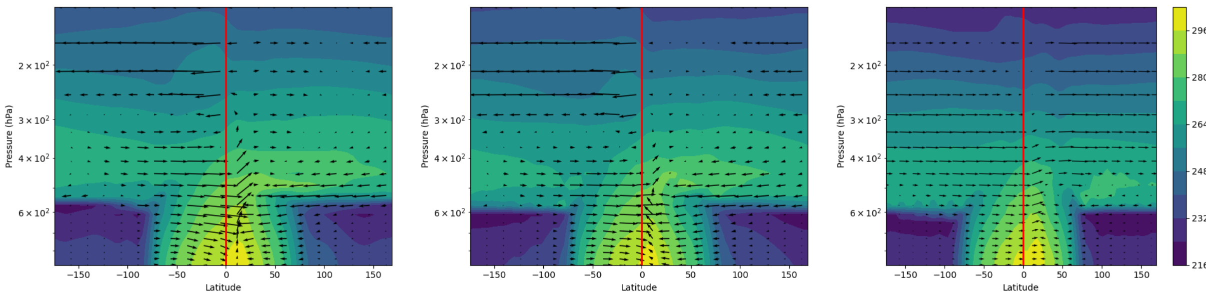

(a) 1 m (b) 0.1 m (c) 0.01 m

Figure 3.4: Zonal cross-section of temperature and winds at the equator. The substellar point is marked by the solid red line.

The equatorial zonal cross-section of the wind profile, as shown in Figure 3.4, shows strong convection originating from the day side – crossing the 500 hPa level (above the night-side boundary layer inversion height). An interesting thing of note is that in the 0.01m run, the rising air appears to have an almost exclusively westerly tendency (which manifests as the equatorial westerly flow in the mid-tropospheric region of about 200 to 500 hPa), while in the 0.1m and 1m runs, the rising air appears to gain an easterly tendency as it continues to rise (Figure 3.4).

It is also apparent from Figure 3.4 that in the 0.01m run, the winds in both the eastern and western sides of the substellar point are of almost uniform speeds whereas in the 0.1m and 1m runs, the eastern and western hemispheres (centred around the substellar point) have very unequal and opposing winds. The eastern hemisphere especially seems to have very low wind speeds compared to the western hemisphere. This contrast between the runs is most apparent in the 500 to 200 hPa levels. Above the 200/250 hPa level, all three cases show the same feature of having opposing and unequal wind speeds although the pattern of winds are different between the 0.01m run and the 1m and 0.1m runs. These asymmetries in the climatology could be indicative of strong stationary wave activity in the troposphere. This will be explored more in the next chapter.

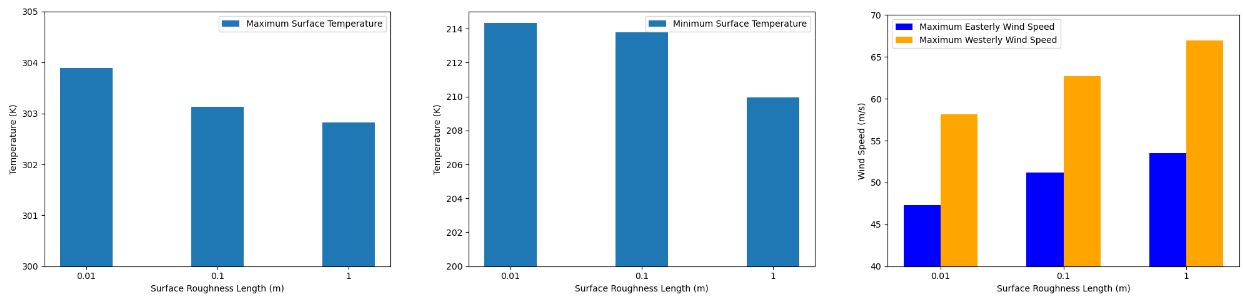

Figure 3.5: Inter-run comparisons of maximum and minimum surface temperatures, and absolute windspeeds (easterly and westerly) in 5-year climatologies of each run

The Outgoing Longwave Radiation (OLR) plays an important role in the phase-curve mapping used by astronomers and modellers alike to identify the coarse circulation features of an exoplanetary system. We can see the changes in OLR with changing surface roughness length in Figure 3.6 below.

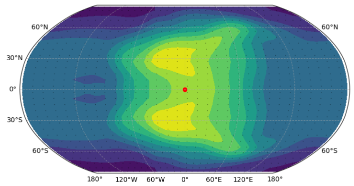

(a) 1 m

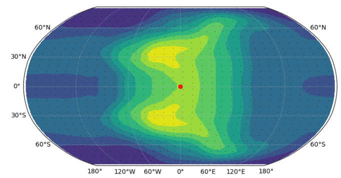

(b) 0.1 m

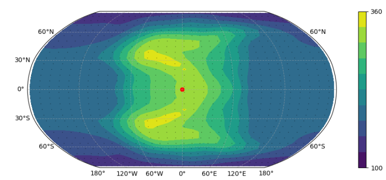

(c) 0.01 m

Figure 3.6: Outgoing Longwave Radiation (in W/m^2). Red dot marks the substellar point

Chapter 4

Eddy-Driven Circulation

Considering the atmosphere as a turbulent fluid, fluctuations in field variables such as wind speeds, temperature, etc., can be attributed to the action of waves and turbulent swirls of motion called eddies (Holton and Hakim 2013, Stull 2012). Reynolds decomposition of the total wind fields allow us to study the effects of the mean wind flow and the deviations or perturbations from the mean, i.e., eddies. Since eddies are very important in transporting momentum in the atmosphere, we hope to explore their contributions in maintaining the circulation in our model by estimating the eddy momentum fluxes and their profiles.

4.1 Influence of Eddies on Momentum Fluxes

Understanding the transport of zonal momentum is crucial in understanding the differences in circulation features of these runs. For this, we have to look at the transport of zonal momentum by the mean flow, stationary and transient eddies. This can help us identify the dominant factors in modulating the circulation regimes we have modelled.

The momentum flux by stationary eddies can be calculated as the deviations from the zonal mean of the climatological winds.

$$u^* = u - \overline{u} \tag{4.1}$$
$$v^* = v - \overline{v} \tag{4.2}$$

where the overbar stands for the zonal mean and the star shows the stationary eddy components.

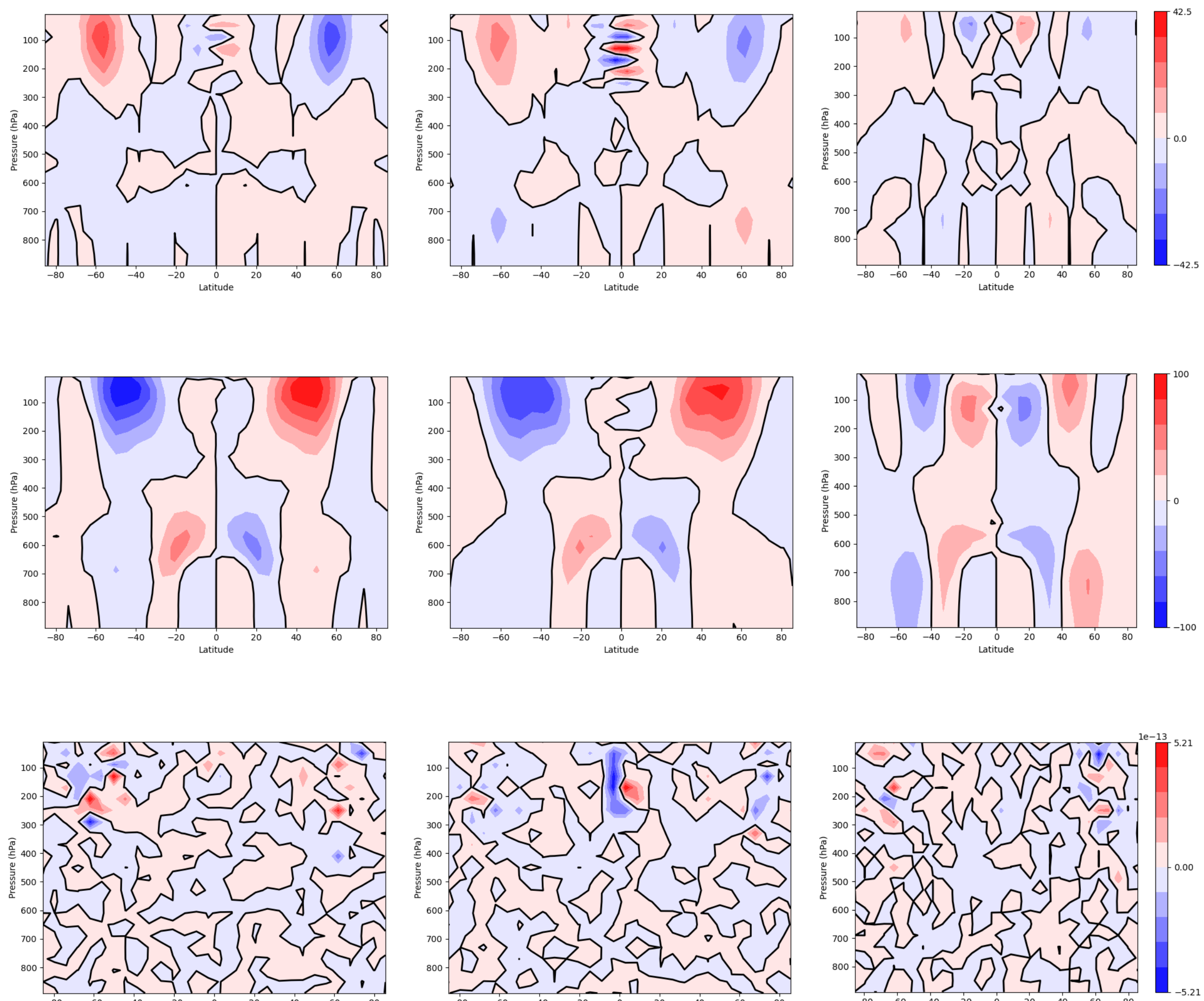

(a) 1 m (b) 0.1 m (c) 0.01 m

Figure 4.1: Meridional fluxes of zonal momentum by mean-flow (top), stationary waves (middle), and transient eddies (bottom)

This gives us the meridional flux of the zonal momentum by stationary eddies as $u'v'$. Similarly the vertical fluxes can be calculated as $u'w'$ for the vertical transport.

The transient eddy contributions $u'v'$ are calculated as the remainder of the zonal mean and the stationary eddy components from the total field.

$$u' = u - [\overline{u}] - u^* \tag{4.3}$$
$$v' = v - [\overline{v}] - v^* \tag{4.4}$$

where the [.] represents the time averaging operator.

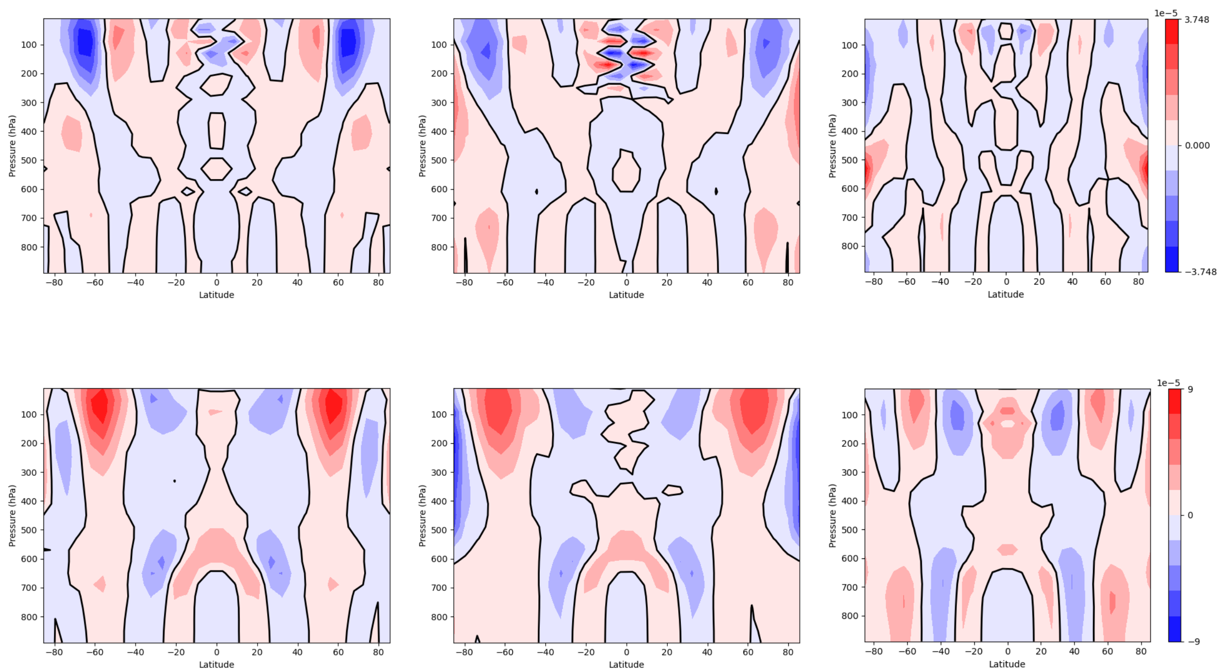

(a) 1 m (b) 0.1 m (c) 0.01 m

Figure 4.2: Divergence of meridional fluxes of zonal momentum by mean-flow (top), and stationary waves (bottom)

Figure 4.1 shows the fluxes of momentum by the mean flow, stationary and transient eddies and their divergences - which can help identify where the fluxes add or remove momentum from the zonal mean flow. The meridional transport of zonal momentum by the mean flow, while comparable in order to the stationary eddy fluxes, are not as strong as the stationary eddies in magnitude. We can clearly infer that the magnitude, and thus the influence, of the transient eddies on transporting zonal momentum to be very small. Hence we can neglect the influence of the transient eddies on supporting the circulation from the analyses to come. The problem is evidently dependent on the stationary eddy fluxes and their behaviour and so we shall focus on the stationary eddy behaviour in our analyses.

We can calculate the stationary eddy flux divergence (or Reynolds Stress S) as (Caballero and Anderson 2009):

$$S_{st} = -\frac{1}{a\cos^2\varphi}\frac{\partial}{\partial\varphi}\left(\cos^2\varphi\,[\overline{u^*v^*}]\right) \tag{4.5}$$

The meridional stationary eddy fluxes of zonal momentum appears to increase in magnitude in the mid-latitude regions. Examining their divergences (Figure 4.2) as well shows that there is an increased deposition of positive zonal momentum (which implies strengthening of westerlies) in the mid-latitude upper troposphere as the roughness length increases. The magnitude of the meridional fluxes in the mid-latitude regions also increases proportional to the surface roughness. This is also visible in the wind profiles earlier examined. Hence we can infer that the stationary waves help strengthen the mid-latitude westerlies as the surface friction increases.

Showman and Polvani 2010 shows that the effect of vertical transport of angular momentum is important in sustaining an equatorial super-rotating jet when a system is subjected to longitudinally varying heating (which is similar to our forcing condition). While the equatorial westerly flow observed in the zonal-mean zonal winds (Figure 3.3-c) is not a super-rotating jet (since the flow is not zonally symmetric - Figure 3.4-c) in our case, it is still relevant to analyze the vertical momentum transport. This zonal asymmetry can be attributed to the strong Matsuno-Gill response dominating the mid-troposphere atmosphere

(Figure 4.5). So we can check the vertical transport of zonal momentum by stationary eddies as u^*w^*. This value can be differentiated with the pressure levels (and scaled by the acceleration due to gravity) to obtain the divergence as:

$$\text{Vertical Stationary Eddy Stress} = -g\frac{d(u^*w^*)}{dP} \tag{4.6}$$

Due to the chosen resolution of the horizontal grids being low, the value of the vertical wind speeds obtained from the continuity equation is generally one (or more) orders of magnitudes lower than that of the horizontal winds. This is reflected in the vertical stationary eddy fluxes being computed to be smaller than the meridional stationary eddy fluxes of zonal momentum (Figure 4.1, 4.3).

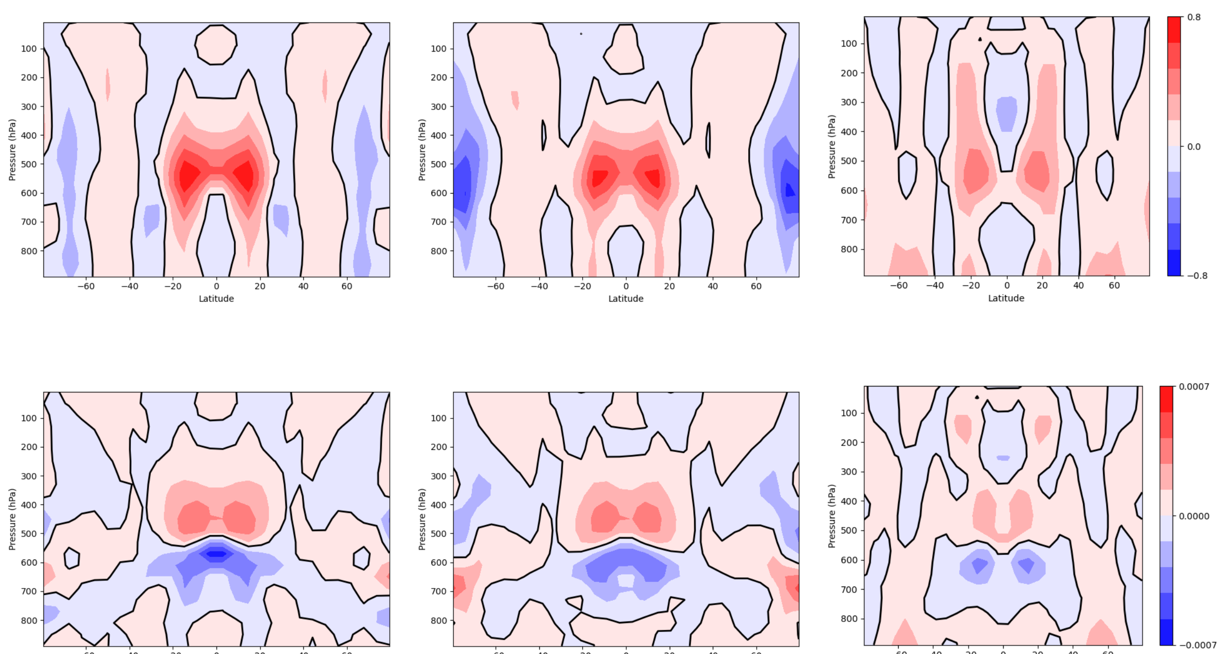

(a) 1 m (b) 0.1 m (c) 0.01 m

Figure 4.3: Vertical flux of zonal momentum by stationary eddies (top) in and the corresponding divergence (bottom)

On comparing the divergences of the vertical stationary eddy flux, we can see an increasing easterly momentum tendency in the lower troposphere with increasing surface roughness while the mid-tropospheric westerly tendency seems to increase from the 0.01m to the 0.1m run and remains constant for the 1m case. However, it is to be noted that the magnitude of the vertical flux of zonal momentum increases steadily as the surface roughness increases.

To better understand the full zonal momentum balance better, we need to examine the effects of the vertical flux of zonal momentum by mean winds and the effects of the Coriolis term as well. In flux form, the zonally averaged zonal momentum balance can be expressed as:

$$\frac{\partial \overline{u}}{\partial t} = -\frac{1}{a\cos\phi}\frac{\partial}{\partial \phi}\left(\overline{uv}\cos\phi\right) - \frac{\partial}{\partial p}\left(\overline{u\omega}\right) + f\,\overline{v} - \overline{X} \tag{4.7}$$

where X represents the frictional or other external influences to zonal momentum. On decomposing the winds into the zonal mean and stationary eddy components (we have established that the transient eddies have negligible effects on the circulation), the equation takes the following form:

$$\frac{\partial \overline{u}}{\partial t} = -\frac{1}{a\cos\phi}\frac{\partial}{\partial \phi}\left[\left(\overline{u}\,\overline{v} + \overline{u^* v^*}\right)\cos\phi\right] - \frac{\partial}{\partial p}\left(\overline{u}\,\overline{\omega} + \overline{u^* \omega^*}\right) + f\,\overline{v} - \overline{X} \tag{4.8}$$

Hence, the Coriolis term and the vertical flux of zonal momentum by mean winds are necessary to give insights into the momentum balance at play in our model and for us to infer the effects of drag and diffusion on the system. Figure 4.4 shows the vertical flux of zonal momentum by mean winds to behave similarly to the behaviour of the vertical flux by stationary eddies. Figure 4.5 depicts the Coriolis term and it shows strongly non-linear inter-run trends in the mid-latitude lower troposphere with the easterly acceleration being strongest in the 0.1 m run. Exclusive analysis of the momentum tendencies induced by the PBL component is necessary and I hope to better understand the effects of drag and diffusion in the future.

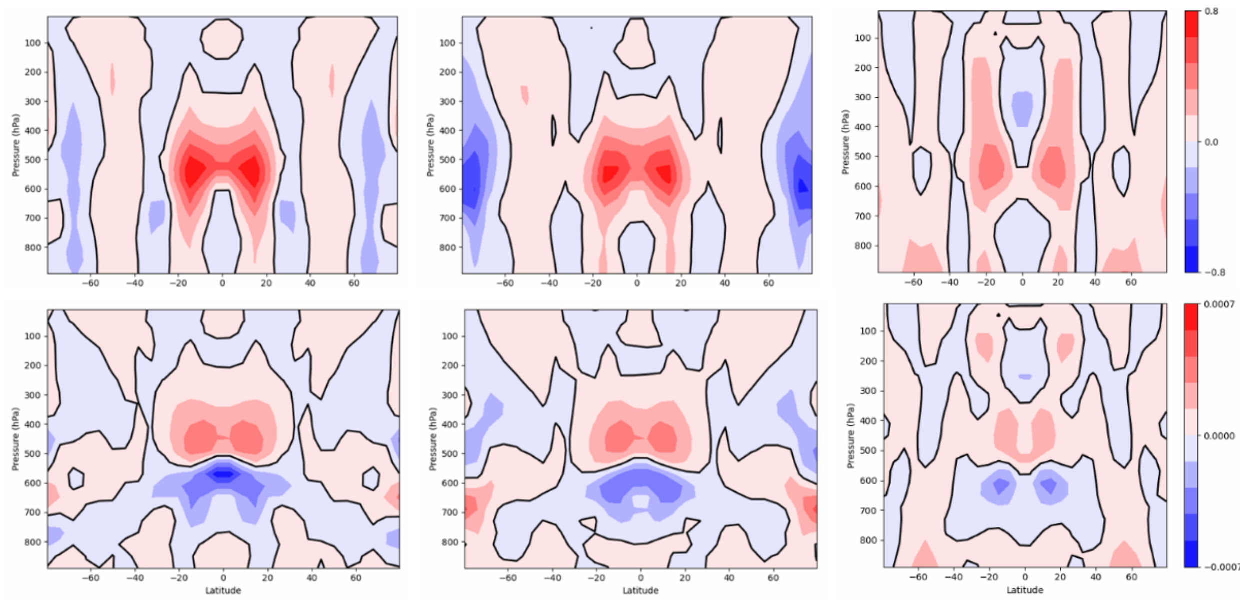

(a) 1 m (b) 0.1 m (c) 0.01 m

Figure 4.4: Vertical flux of zonal momentum by mean winds (top) in and the corresponding divergence (bottom)

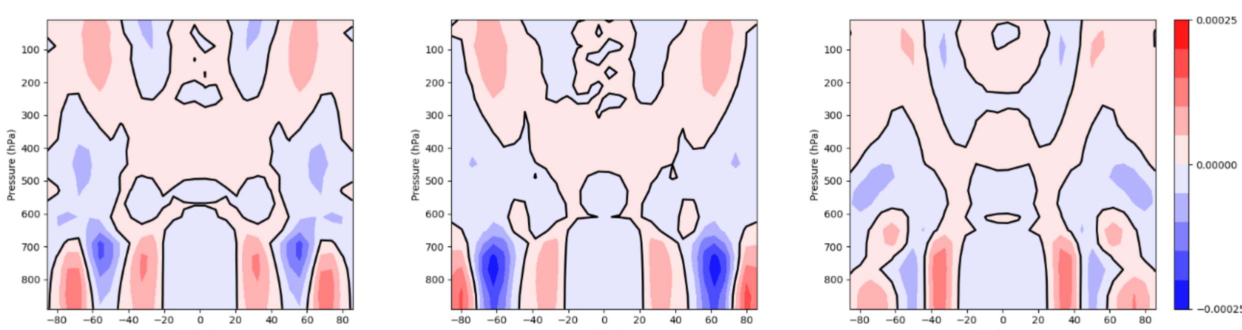

(a) 1 m (b) 0.1 m (c) 0.01 m

Figure 4.5: The Coriolis term ($-fv$) in m/s^2

4.2 Stationary Wave Response and Vorticity Budgets

Since the dominant effects on the circulation are from the stationary waves, we can slice into the isobaric pressure levels along the jet cores (at approximately 170 hPa) to look at the stationary wave response and how it supports the wind profiles (Figure 4.6 and Figure 4.7).

The alternating positive and negative geo-potential anomaly between the day and night side suggests strong large-scale planetary wave activity. A strong Matsuno-Gill response is visible in the mid-tropospheric region at about 500 hPa (Figure 4.6) with a Kelvin response east of the substellar point (at 0^o longitude and 0^o latitude as seen in Figure 2.4). At the 170 hPa level, a modified response with the presence of a Kelvin wave along the equator and multiple Rossby gyres in the higher latitudes can be observed in all the 3 cases (Figure 4.6). The meridional extent of the gyres and the stationary eddy geo-potential anomalies should be noted– in that the wave response is restricted to the tropics in the low surface roughness length run of 0.01m while in the other cases, it can be seen to extend to the higher latitudes. This is evident in both Figure 4.6 and 4.7. Monteiro, Adames, et al. 2014 and Lau and Lim 1984 suggest that the changes in background zonal mean flow is responsible for this change in behaviour. The increasing westerly tendency as one move poleward from the equator in the 1m and 0.1m runs causes the Rossby wave trains to be unrestricted by the equatorial waveguide. The presence of a mean westerly equatorial flow in the 0.01m run (Figure 3.3-c) creates an easterly shear which inhibits the meridional propagations of the wave trains.

There also appears to be strongly divergent flow at the equatorial region of the 0.01m run. We can try to understand the vorticity balance in such a profile using a barotropic vorticity equation in a steady state and linearized about the mean winds (Monteiro, Adames, et al. 2014) as:

$$(f - \partial_y \bar{u})\nabla \cdot \mathbf{u}' + v' \partial_y (f - \partial_y \bar{u}) + \bar{u} \partial_x \zeta' = 0. \tag{4.9}$$

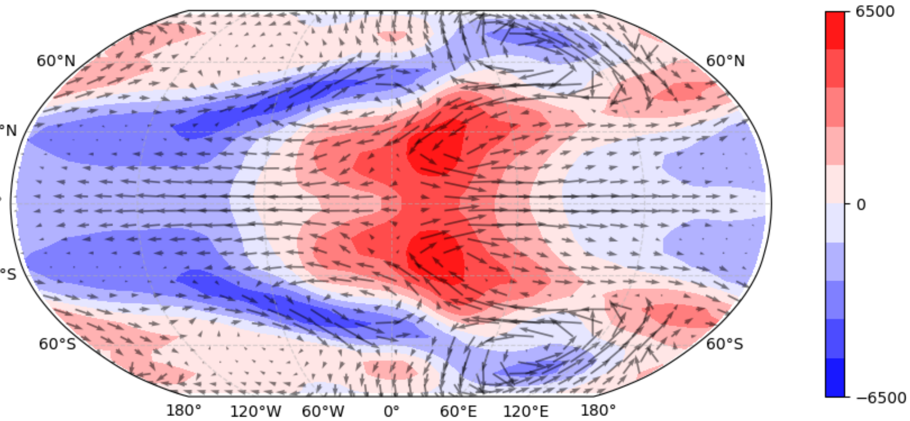

(a) 1 m

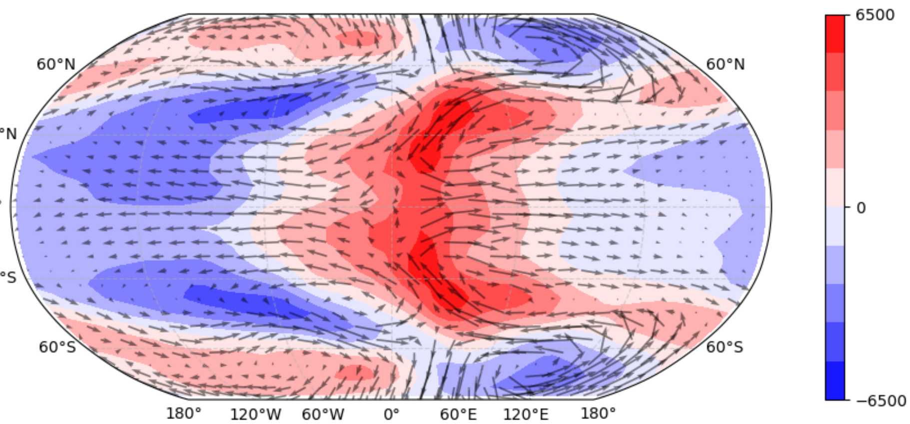

(b) 0.1 m

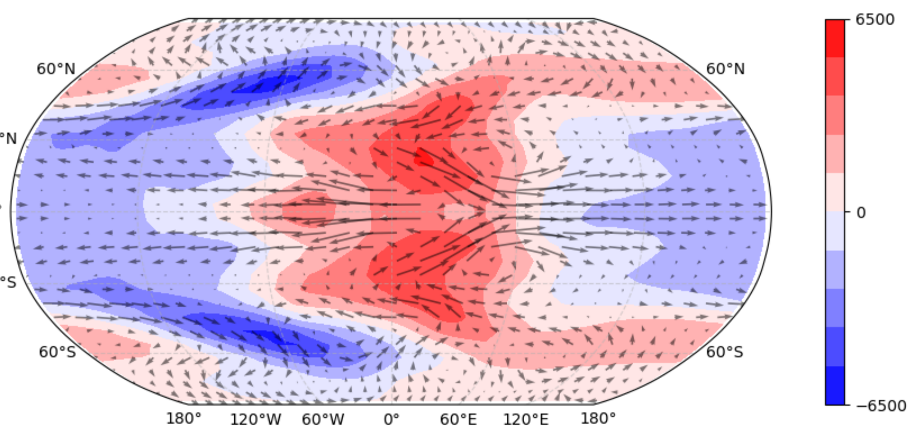

(c) 0.01 m

Figure 4.6: Stationary wave responses at the 170 hPa level. Contoured are the geopotential anomaly (m^2/s^2)

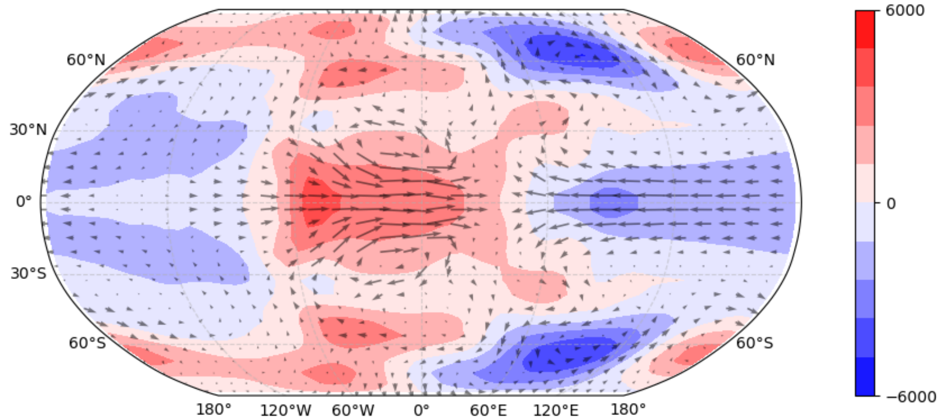

(a) 1 m

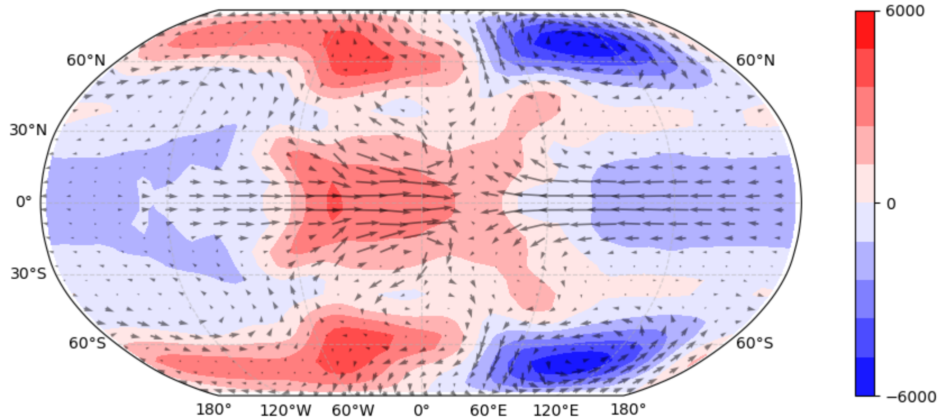

(b) 0.1 m

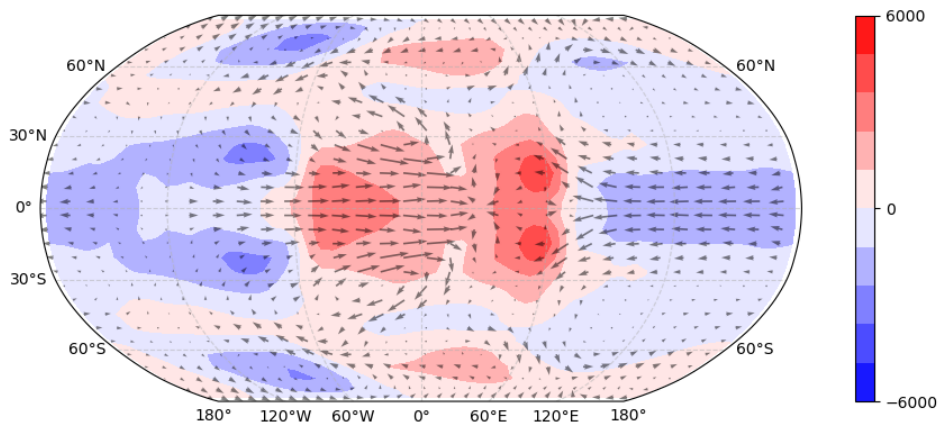

(c) 0.01 m

Figure 4.7: Stationary wave responses at the 490 hPa level. Contoured are the geopotential anomaly (m^2/s^2)

where ζ' stands for the eddy relative vorticity.

Essentially this gives us 3 terms that could potentially give a sense of the vorticity balance (excluding external forcing). Term 1 represents the vorticity generation due to divergence, term 2 represents the meridional advection of planetary vorticity and term 3 represents the advection of the eddy relative vorticity by zonal-mean zonal winds. We can plot each of these terms for each case to find the balance of vorticity in the lower latitudes. Since the magnitude of planetary vorticity increases with latitude, for the purpose of visualization we will limit the meridional extent of our plots to 45^o N-S. This can help highlight the vorticity balance in the lower latitudes.

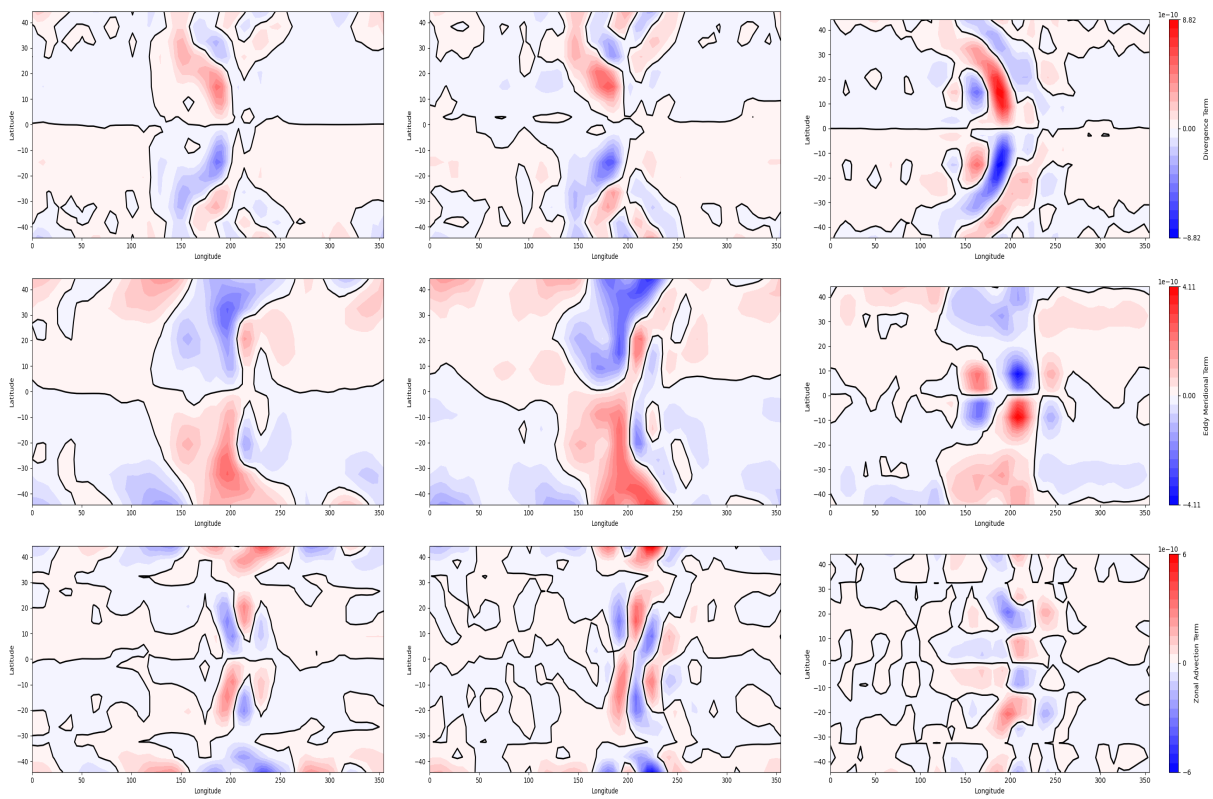

(a) 1 m (b) 0.1 m (c) 0.01 m

Figure 4.8: Barotropic vorticity balance terms. The top row shows vorticity generation by divergence (Term 1), middle row shows meridional advection of planetary vorticity (Term 2) and the eddy relative vorticity advection by zonal mean zonal winds (Term 3) in the bottom row

Figure 4.8 shows that the divergence term (Term 1) in the lower latitudes (20N to 20S extent) appears to get weaker with increasing roughness length and is predominantly balanced by the meridional advection of planetary vorticity (Term 2). The advection of eddy relative vorticity by zonal-mean zonal winds appear to be a much smaller balancing factor (Term 3). The non-linearity of the vorticity terms between the three surface roughness cases should be noted, particularly for Term 2 and Term 3.

The dominant generation of vorticity by divergence and the apparent Kelvin wave signatures in the upper troposphere prompts us to examine the zonal circulation in detail. This can be done by calculating the zonal mass streamfunction averaged in the 30N-30S meridional extent (Figure 4.9). The mass streamfunction can be calculated from the continuity equation balanced between the zonal gradient of the zonal wind speeds (averaged over the 30 N-S range to account for any meridional mass fluxes into or out of the region) and the pressure gradient of the vertical winds.

$$\frac{\partial u}{\partial x} + \frac{\partial w}{\partial p} = 0 \tag{4.10}$$

where the value of u is taken as the meridional average between our chosen latitude extend (averaged with $cos\phi$ weightage).

$$u = -\frac{\partial \Psi_x}{\partial p} \tag{4.11}$$

$$w = \frac{\partial \Psi_x}{\partial x} \tag{4.12}$$

Thus the mass streamfunction ϕ can be calculated as:

$$\Psi_x(x,p) = \int_p^{p_s} w\,dp' \tag{4.13}$$

We examine the streamfunction for both the total flow and the eddy flow for the climatologies of all three runs.

The total mass streamfunction profile (Figure 4.9, top row) shows quite a considerable difference between the 0.01m run and the rest. In the 0.01m run, we can observe closed clockwise (positive) and counter-clockwise (negative) overturning Walker-like circulations in the zonal direction. However, in the higher surface roughness runs, there are very few closed contours and while the magnitude of the negative streamfunctions increases, a majority of the contours are discontinuous indicating a mass imbalance at the surface.

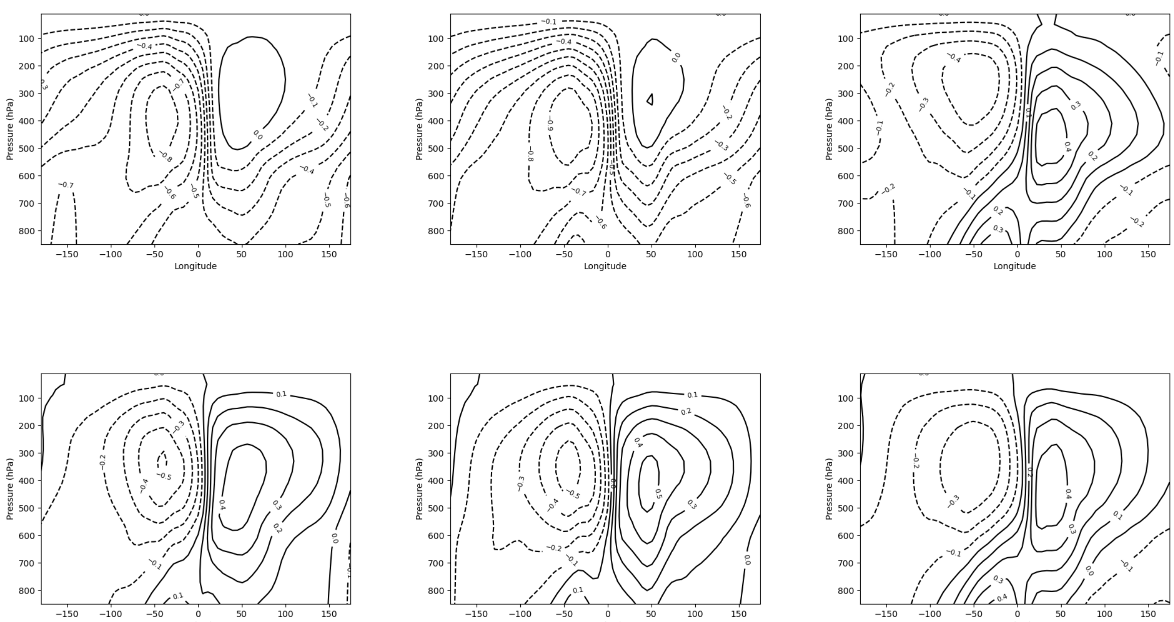

(a) 1 m (b) 0.1 m (c) 0.01 m

Figure 4.9: Zonal mass streamfunctions averaged over the 30 N-S extent. The top row shows the total mass streamfunction and the bottom row shows the eddy mass streamfunctions

On reviewing the zonal mass streamfunctions for the stationary eddies calculated over the same meridional extent (Figure 4.9, bottom row), we find much more uniform profile characteristics between the runs. There are strong overturning circulations in both western and eastern sides of the substellar point and the magnitude of the streamfunctions increase from the 0.01m run to the 0.1 and 1m runs. It appears to suggest a mild asymmetry in the strength of the circulations with the clockwise overturning circulation to the east of the substellar point to be slightly stronger than the counter-clockwise circulation in the west.This asymmetry is caused by the eastern overturning circulation being a Kelvin wave driven response while the western circulation is likely thermally driven.

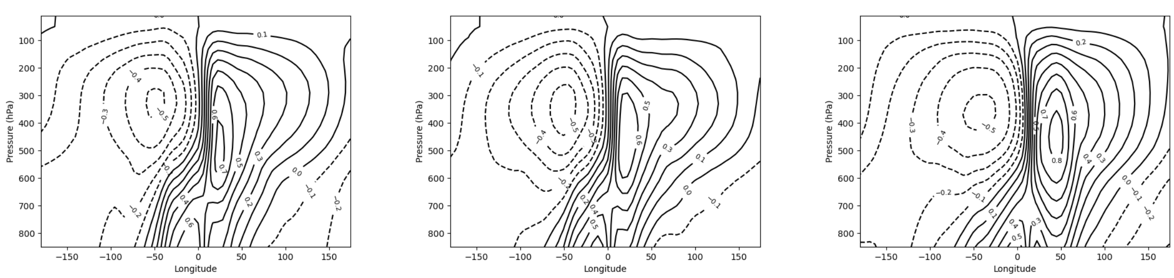

(a) 1 m (b) 0.1 m (c) 0.01 m

Figure 4.10: Zonal eddy mass streamfunctions averaged over the 20 N-S extent.

Chapter 5

Conclusion

From the previous discussions, some conclusions can be drawn with the available data and the analyses performed.

The most notable feature is the shift of the equatorial flow from a strong mid-tropospheric westerly core to an easterly mean flow as the surface roughness is increased. Such a result can have implications in shift of the exoplanetary hotspot in its mapped phase curve (Lichtenberg and Miguel 2024, Kreidberg et al. 2019, Demory et al. 2016). We hope to explore this in detail in the future.

The influence of transient eddies appear to be significantly smaller than that of stationary eddies in driving the circulation. This reduces the problem to that of quantifying how changing surface roughness length changes the stationary eddies. It is also clear that the meridional flux of zonal momentum by stationary waves has a stronger impact than the transport of zonal momentum by the mean flow. More analyses, especially for the transience between the different surface roughness conditions, need to be considered to fully understand the dynamics at play here.

The general features of the changes in circulation is in agreement with Chen et al. 2007 in that the subtropical jets shift equatorward with increasing friction. This, along with the change in the easterly or westerly tendency as one moves poleward from the equator, causes the stationary wave profiles to become increasingly independent of the equatorial waveguide as shown by Monteiro, Adames, et al. 2014 and Lau and Lim 1984.

A major portion of the project was spent on understanding the boundary layer behaviour and implementing a newer version which can help sustain a tidally-locked atmosphere. In this pursuit, quite a number of important concepts, modelling techniques, their advantages and disadvantages, and their physical implications were understood. The PBL drag should ideally be formulated asymptotically to the stability parameter (Richardson number in our case) to avoid energetic decoupling between the atmosphere and the surface in conditions of extreme stability. Parameterization of often-neglected non-turbulent phenomenon (such as cold air drainage) which could become prominent in conditions of extreme stability could also help make the model more realistic. It is to be noted that since the behaviour of the PBL in conditions of high and prolonged stability is still not well studied and fully understood, more work needs to be done on this topic to allow for a more accurate simulation of tidally-locked exoplanetary atmosphere. Nonetheless, given that the modelled behaviour of eddies and jets correlate well with other studies on the effect of friction on atmospheric circulation shows that we have been able to develop a reasonable and simple model to study the dynamics of a tidally-locked atmosphere.

References

Blackadar, Alfred K (1962). "The vertical distribution of wind and turbulent exchange in a neutral atmosphere". In: *Journal of Geophysical Research* 67.8, pp. 3095–3102.

Caballero, Rodrigo and Bruce T Anderson (2009). "Impact of midlatitude stationary waves on regional Hadley cells and ENSO". In: *Geophysical research letters* 36.17.

Carson, DJ and PJR Richards (1978). "Modelling surface turbulent fluxes in stable conditions". In: *Boundary-Layer Meteorology* 14.1, pp. 67–81.

Chen, Gang, Isaac M Held, and Walter A Robinson (2007). "Sensitivity of the latitude of the surface westerlies to surface friction". In: *Journal of the atmospheric sciences* 64.8, pp. 2899–2915.

Crossfield, Ian J. M. (Oct. 2015). "Observations of Exoplanet Atmospheres". In: *Publications of the Astronomical Society of the Pacific* 127.956, p. 941. DOI: 10.1086/683115. URL: https://dx.doi.org/10.1086/683115.

Demory, Brice-Olivier et al. (2016). "A map of the large day–night temperature gradient of a super-Earth exoplanet". In: *Nature* 532.7598, pp. 207–209.

Emanuel, Kerry A and Marina Živković-Rothman (1999). "Development and evaluation of a convection scheme for use in climate models". In: *Journal of the Atmospheric Sciences* 56.11, pp. 1766–1782.

Feinstein, Adina D et al. (2023). "Early Release Science of the exoplanet WASP-39b with JWST NIRISS". In: *Nature* 614.7949, pp. 670–675.

Frierson, Dargan MW, Isaac M Held, and Pablo Zurita-Gotor (2006). “A gray-radiation aquaplanet moist GCM. Part I: Static stability and eddy scale”. In: *Journal of the atmospheric sciences* 63.10, pp. 2548–2566.

Holton, James R and Gregory J Hakim (2013). *An introduction to dynamic meteorology.* Vol. 88. Academic press.

Hu, Yongyun and Jun Yang (2014). “Role of ocean heat transport in climates of tidally locked exoplanets around M dwarf stars”. In: *Proceedings of the National Academy of Sciences* 111.2, pp. 629–634.

Kondo, J, O Kanechika, and N Yasuda (1978). “Heat and momentum transfers under strong stability in the atmospheric surface layer”. In: *Journal of Atmospheric Sciences* 35.6, pp. 1012–1021.

Kreidberg, Laura et al. (2019). “Absence of a thick atmosphere on the terrestrial exoplanet LHS 3844b”. In: *Nature* 573.7772, pp. 87–90.

Lau, Ka-Ming and Hock Lim (1984). “On the dynamics of equatorial forcing of climate teleconnections”. In: *Journal of Atmospheric Sciences* 41.2, pp. 161–176.

Lichtenberg, Tim and Yamila Miguel (2024). “Super-Earths and Earth-like exoplanets”. In: *arXiv preprint arXiv:2405.04057*.

Long, Paul E (1986). “An economical and compatible scheme for parameterizing the stable surface layer in the medium range forecast model”. In.

Louis, Jean-François (1979). “A parametric model of vertical eddy fluxes in the atmosphere”. In: *Boundary-Layer Meteorology* 17.2, pp. 187–202.

Madhusudhan, Nikku et al. (2014). “Exoplanetary atmospheres”. In: *arXiv:1402.1169*.

Monin, Andreı Sergeevich and Aleksandr Mikhaılovich Obukhov (1954). “Basic laws of turbulent mixing in the surface layer of the atmosphere”. In: *Contrib. Geophys. Inst. Acad. Sci. USSR* 151.163, e187.

Monteiro, Joy M, Ángel F Adames, et al. (2014). “Interpreting the upper level structure of the Madden-Julian oscillation”. In: *Geophysical Research Letters* 41.24, pp. 9158–9165.

Monteiro, Joy Merwin, Jeremy McGibbon, and Rodrigo Caballero (2018). "sympl (v. 0.4. 0) and climt (v. 0.15. 3)–towards a flexible framework for building model hierarchies in Python". In: *Geoscientific Model Development* 11.9, pp. 3781–3794.

Pierrehumbert, Raymond T and Mark Hammond (2019). "Atmospheric circulation of tide-locked exoplanets". In: *Annual Review of Fluid Mechanics* 51.1, pp. 275–303.

Seidel, Julia V, Louise D Nielsen, and Subhajit Sarkar (2023). *JWST opens a window on exoplanet skies*.

Showman, Adam P and Lorenzo M Polvani (2010). "The Matsuno-Gill model and equatorial superrotation". In: *Geophysical Research Letters* 37.18.

Stull, Roland B (2012). *An introduction to boundary layer meteorology*. Vol. 13. Springer Science & Business Media.

Vallis, Geoffrey K (2017). *Atmospheric and oceanic fluid dynamics*. Cambridge University Press.

Virtanen, Pauli et al. (2020). "SciPy 1.0: Fundamental Algorithms for Scientific Computing in Python". In: *Nature Methods* 17, pp. 261–272. DOI: 10.1038/s41592-019-0686-2.

Wallace, John M et al. (2023). *The Atmospheric General Circulation*. Cambridge University Press.

Wieringa, Jon (1992). "Updating the Davenport roughness classification". In: *Journal of Wind Engineering and Industrial Aerodynamics* 41.1-3, pp. 357–368.

Zheng, Weizhong et al. (2017). "Improving the stable surface layer in the NCEP global forecast system". In: *Monthly Weather Review* 145.10, pp. 3969–3987.